Supplemental Information

Table S1. qRT-PCR primers and shRNA sequences.

Figure S1. The expanded lipidomic composition of sea urchin and mammalian LLC-PK1 cilia.

HPLC-MS/MS quantification and chromatograms of diverse sterols from ciliated sea urchin embryos (**A, B**) and LLC-PK1 cells (**C, D**).

(*) = $P \leq 0.05$, Student's t test.

See also Figure 1 and Figure 4.

Figure S2. Cilia-associated oxysterols cause SMO to accumulate in cilia and activate the HH pathway through the CBP.

(**A**) Ciliary (ARL13B, red) and nuclear (DAPI, blue) immunofluorescence of NIH/3T3 cells stably expressing mouse SMO-EGFP or SMO^{Y134F}-EGFP treated with vehicle (ethanol) or 30 μM 7β,27-OHC or 24(*S*),25-EC 30 μM. Cilia-associated oxysterols cause SMO to accumulate in cilia. Y134F substitution in the CRD blocks the effect of 7β,27-OHC but not 24(*S*),25-EC on ciliary accumulation. Scale bars: main, 10μm; insert, 1μm.

(**B**) Cilia-associated oxysterol probe synthesis. Copper(II) sulfate pentahydrate, CuSO4 5H2O; dichloromethane, DCM; 4-dimethylaminopyridine, DMAP; N,N'-dimethylformamide, DMF; ethynylmagnesium bromide, HCCMgBr; lithium aluminum hydride, LAH; manganese dioxide, MnO_2; pyridinium chlorochromate, PCC; tert-butyldimethylsilyl chloride, TBS-Cl; tetrahydropyran, THF; and tetra-n-butylammonium, TBAF.

(**C**) Ciliary (ARL13B, red) and nuclear (DAPI, blue) immunofluorescence of NIH/3T3 cells stably expressing mouse SMO-, SMO^{D259R}-, SMO^{N450D} -, or $SMO^{Y134F, D259R}$-EGFP. Substitutions of the CBP, and combined substitution in the CRD and CBP, block SMO accumulation in cilia. Scale bars: main, 10μm; insert, 1μm.

(**D**) Luciferase activity of ciliated $Smo^{-/-}$ MEFs co-transfected with *Gli*-luciferase reporter and SMO SMOM2 with the indicated substitutions and treated with vehicle (DMSO), 1μg/ml SHH, or 100nM SAG. Data are normalized to luciferase activity of SMO-expressing cells treated with vehicle. Substitution of the CRD and/or CBP attenuates the activity of SHH and SAG.

(**E**) Ciliary (ARL13B, red) and nuclear (DAPI, blue) immunofluorescence of NIH/3T3 cells stably expressing mouse SMOM2-EGFP or $SMO^{Y134F, D259R}$-EGFP. Combined substitutions of the CRD and CBP block SMOM2 accumulation in cilia. Scale bars: main, 10μm; insert, 1μm.
(*) = $P \leq 0.05$, Student's t test.
See also Figure 1 and Figure 2.

Figure S3. Sterol and oxysterol synthases are expressed in HH-pathway associated medulloblastoma, and pharmacologic inhibition of HSD11β2 blocks accumulation of SMO in cilia and HH pathway activation.

(**A**) RNA sequencing of medulloblastomas from P35 *Math1-Cre SmoM2$^{c/wt}$* mice compared to control cerebella of P35 *SmoM2$^{c/wt}$* littermates shows diverse changes in sterol and oxysterol synthase gene expression in HH-pathway associated medulloblastoma.

(**B**) qRT-PCR assessment of *Hsd11β2* expression in P35 control *SmoM2$^{c/wt}$* cerebella and *Math1-Cre SmoM2$^{c/wt}$* medulloblastomas. Data are normalized to expression in control cerebella. *Hsd11β2* expression is 585±45-fold higher in HH-pathway associated medulloblastoma.

(**C**) Immunoblot of equal quantities of protein lysate from human HH (n=2), Group 3 (n=3) and Group 4 (n=3) medulloblastomas shows that HSD11β2 expression is specific to HH-pathway associated medulloblastoma.

(**D**) Re-analysis of human transcriptome data SPR008292 indicates sterol and oxysterol synthases are expressed in all molecular subgroups of human medulloblastoma. Data are shown in arbitrary units.

(**E**) Immunoblot of lysates from *Ptch1$^{-/-}$* MEFs transduced with scrambled or anti-*Hsd11β2* shRNAs demonstrate of HSD11β2 without altering β-actin expression.

(**F**) Immunofluorescence of endogenous SMO (red) localization to cilia (ARL13B, green) in NIH/3T3 cells treated with vehicle (water), 1μg/ml SHH or 100nM SAG, with or without 400nM CNX. Pharmacologic inhibition of HSD11β2 blocks accumulation of SMO in cilia by SHH or SAG. Scale bar, 1μm.

(**G, H**) Fluorescence of 5nM BODIPY-CYA 5nM (green) and nuclei (Hoechst, blue) in HEK293T cells transfected with SMO and treated with vehicle (DMSA), 50nM CYA or 400nM CNX. Data are normalized to vehicle-treated cells. In contrast to CYA, CNX does not compete with CYA-BODIPY to bind SMO. Scale bar, 10μm.

(**I**) Luciferase activity of ciliated NIH/3T3 cells co-transfected with *Gli*-luciferase reporter and empty vector or HSD11β2 and treated with vehicle (DMSO) or 100nM SAG. Data are normalized to luciferase activity of vehicle-treated cells treated with empty vector. HSD11β2 expression is not sufficient to activate the HH pathway.

(**J**) Luciferase activity of ciliated NIH/3T3 cells co-transfected with *Gli*-luciferase reporter and empty vector or HSD11β2 and treated with 1μg/ml SHH and vehicle (water) or CNX. Data are normalized to maximal activity. HSD11β2 expression increases the IC50 of CNX.

(**K**) qRT-PCR assessment of *Hsd11β2* and *Cyp27a1* expression in ciliated NIH/3T3 and LLC-PK1 cells. Data are shown in arbitrary units. NIH/3T3 cells express *Hsd11β2* and *Cyp27a1,* but LLC-PK1 cells, which do not transduce HH signals, do not express *Cyp27a1*.

(**L**) qRT-PCR assessment of *Hsd11β2* expression in ciliated *Ptch1*$^{-/-}$ MEFs transduced with scrambled control or *Hsd11β2* shRNAs and treated with 1mM MβCD vehicle or 30μM of the indicated oxysterols. Data are normalized to expression in cells transduced with scrambled shRNA and treated with vehicle. *Hsd11β2* knockdown (KD) suppresses *Hsd11β2.*

(**M**) qRT-PCR assessment of *Cyp27a1* expression in ciliated *Ptch1*$^{-/-}$ MEFs transduced with scrambled control or *Cyp27a1* shRNAs and treated with 1mM MβCD vehicle or 30μM of the indicated oxysterols. Data are normalized to expression in cells transduced with scrambled shRNA and treated with vehicle. *Cyp27a1* KD suppresses *Cyp27a1.*

(*) = $P \leq 0.05$, Student's t test.

See also Figures 3 and 4.

Figure S4. The expanded lipidomic composition of medulloblastoma.

(**A**) Sterol mass spectrometry from *SmoM2*^{c} cerebella normalized to sample weight during development (white), adulthood (black) and tumorigenesis (grey and blue).

(**B**) Sterol mass spectrometry normalized to sample weight from P35 *Ptch1*$^{c/c}$ control (black) and *Math1-Cre Ptch1*$^{c/c}$ tumor mice (grey) shows that 7k-C and desmosterol are enriched and 24k-C and 24,25-EC are suppressed in HH-pathway associated medulloblastoma.

(**C**) Cholesterol mass spectrometry normalized to sample weight during development (white), adulthood (black) and in two different genetic models of HH-pathway associated medulloblastoma (grey and blue). In contrast to sterols, cholesterol is suppressed during cerebellar development and tumorigenesis.

(**D**) Oxysterol chromatogram from *Math1-Cre Ptch1*$^{c/c}$ tumor mice.

(*) = P ≤ 0.05, Student's t test.

See also Figure 5.

Figure S5. Pharmacologic inhibition of HSD11β2 blocks oncogenic HH pathway activation.

(**A**, **B**) qRT-PCR assessment of *Mt2* and *Nr3c1 Gli1* expression in P7 and P35 control *Hsd11β2*$^{c/c}$ cerebella, P7 *Math1-Cre SmoM2*$^{c/wt}$ *Hsd11β2*$^{c/c}$ and P35 *Math1-Cre SmoM2*$^{c/wt}$ *Hsd11β2*$^{c/}$medulloblastomas. Data are normalized to expression in control cerebella. Homozygous deletion of *Hsd11β2* does not alter expression of glucocorticoid target genes during cerebellar development or oncogenesis.

(**C**, **D**) Immunofluorescence for apoptotic cells (TUNEL, red) and nuclei (DAPI, blue) from P35 *Math1-Cre Ptch1*$^{c/c}$ medulloblastoma following 14 consecutive days of vehicle (water) or 100μg/g CNX intraperitoneal injection. Pharmacologic inhibition of HSD11β2 does not increase tumor apoptosis, in contrast to glucocorticoid administration (Heine et al., 2011; Heine and Rowitch, 2009). Scale bar, 100μm.

(**E**) qRT-PCR assessment of *Gli1* expression by ciliated ASZ *Ptch1*$^{ko/ko}$ *p53*-mutant mouse basal cell carcinoma cells treated with vehicle (water) or 10μM CNX. Data are normalized to expression in vehicle-treated cells. Pharmacologic inhibition of HSD11β2 blocks oncogenic HH pathway activation in basal cell cancer.

(**F**) qRT-PCR assessment of *Gli1* expression by ciliated Med1 *Ptch1*$^{ko/wt}$ mouse medulloblastoma cells treated with vehicle (water) or 400nM CNX. Data are normalized to expression in vehicle-treated cells. Pharmacologic inhibition of HSD11β2 blocks oncogenic HH pathway activation in medulloblastoma.

(**G**) HPLC-MS/MS measurement of CNX in control P35 *Math1-Cre Ptch1*$^{c/c}$ medulloblastomas 2 hours after intraperitoneal injection of vehicle (water) or 100μg/g CNX. CNX crosses the blood brain barrier.

(**H**) Gross images of P21 control *Ptch1*$^{c/c}$ and *Math1-Cre Ptch1*$^{c/c}$ brains following 14 consecutive days of vehicle (water) or 100μg/g CNX intraperitoneal injection. Pharmacologic inhibition of HSD11β2 attenuates the growth of HH-pathway associated medulloblastoma caused by inactivation of PTCH1. Scale bar, 5mm.

(**I**) Sagittal H&E-stained sections of P21 control *Ptch1*$^{c/c}$ cerebella and *Math1-Cre Ptch1*$^{c/c}$ medulloblastomas following 14 consecutive days of vehicle (water) or 100μg/g CNX intraperitoneal injection. Pharmacologic inhibition of HSD11β2 reduces the number of small round blue tumor cells in HH-pathway associated medulloblastoma. Scale bar, 1mm.

(*) = $P \leq 0.05$, Student's t test.

See also Figure 5.

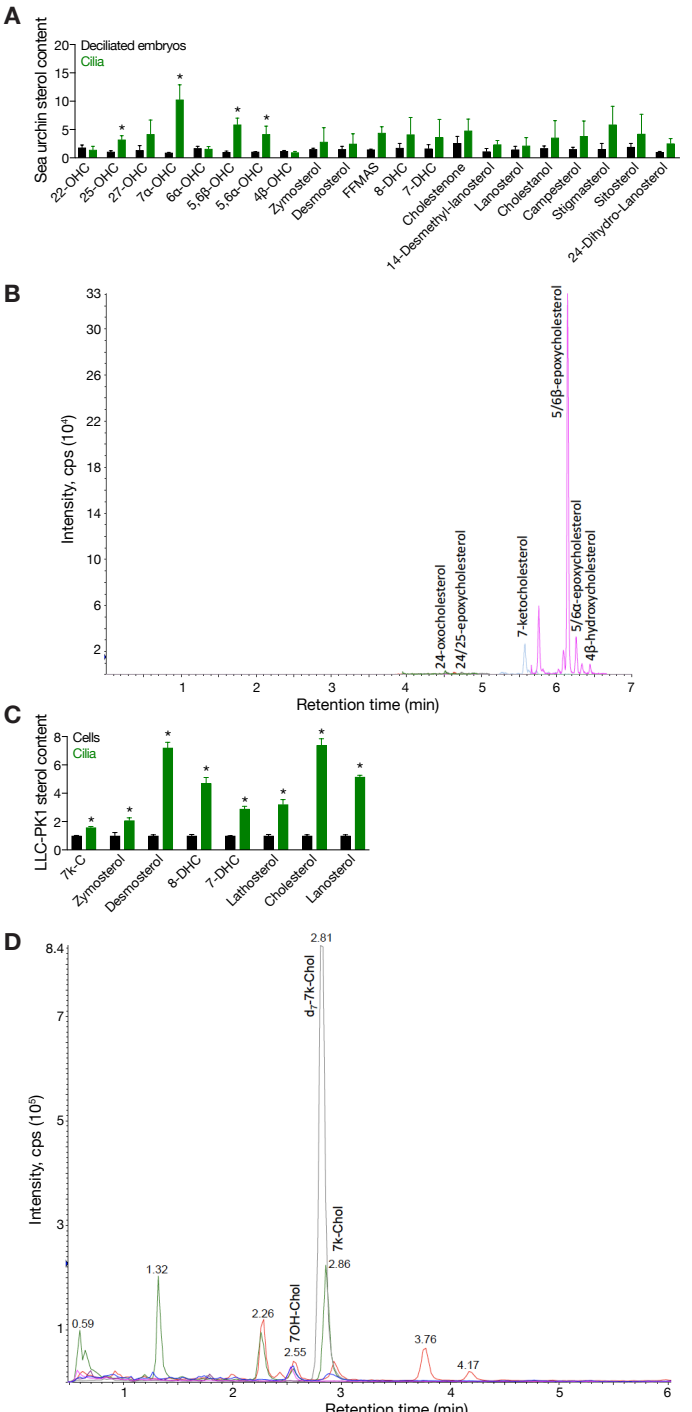

Raleigh et al. Fig. S1

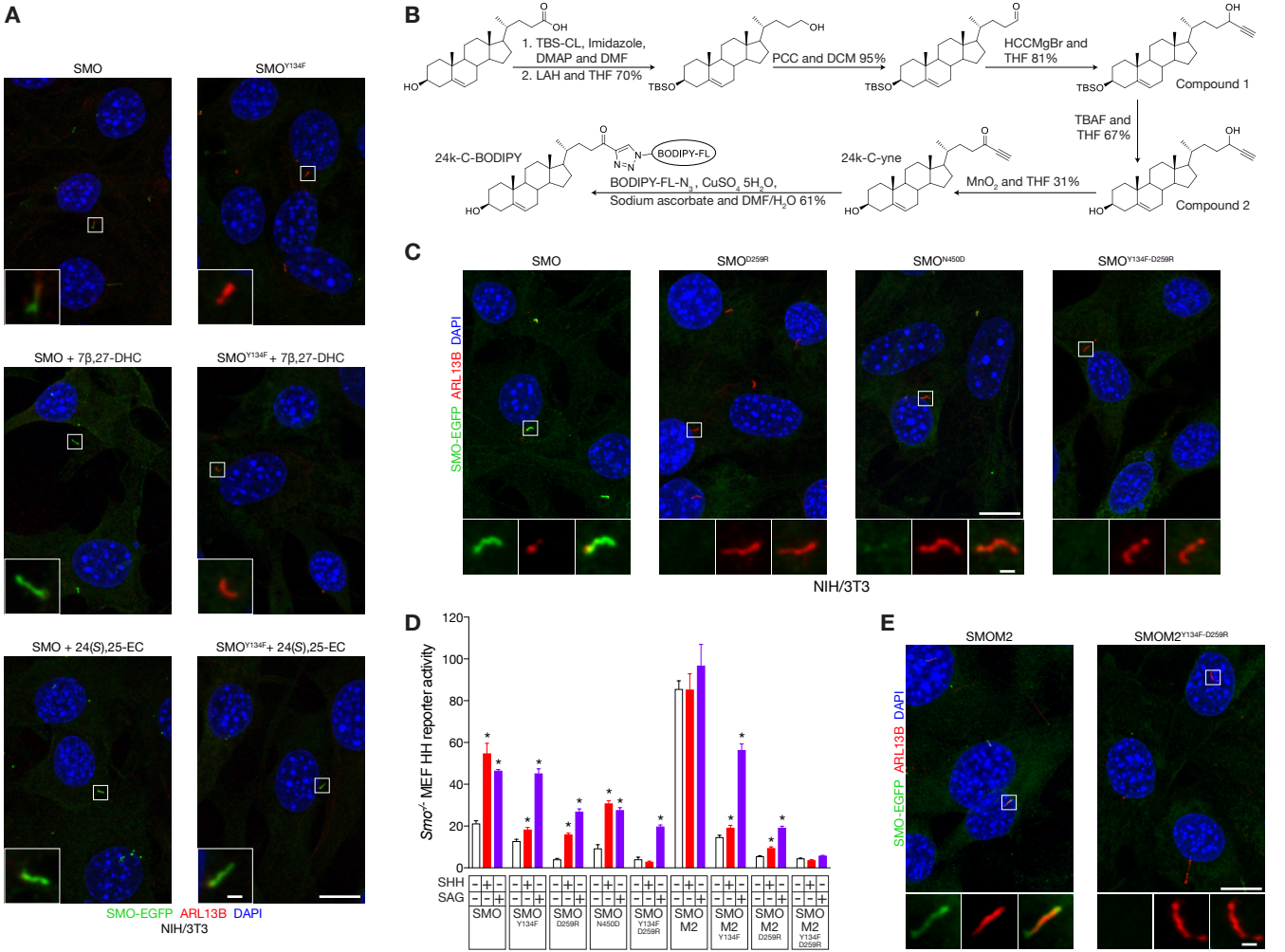

Raleigh et al. Fig. S2

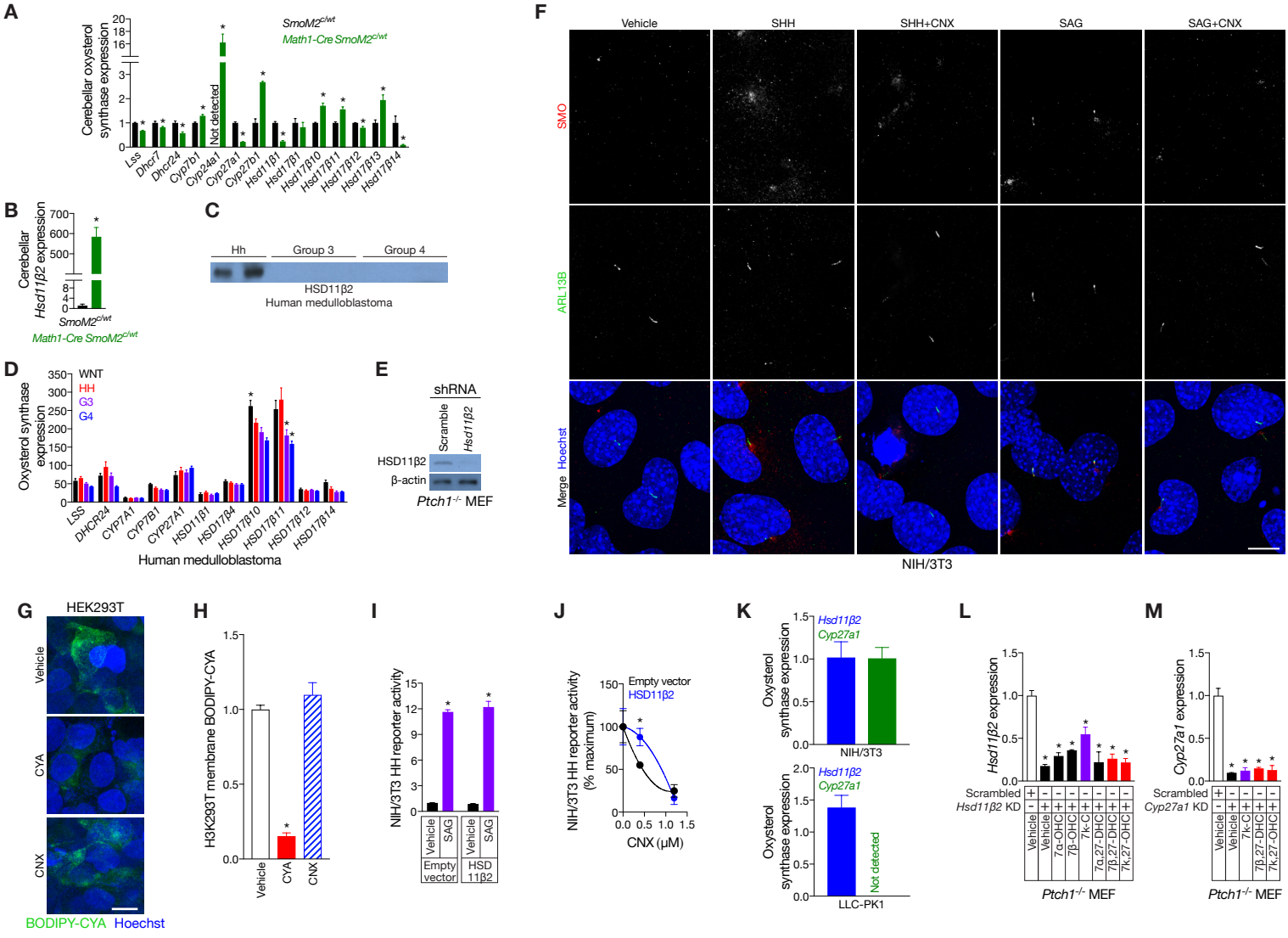

Raleigh et al. Fig. S3

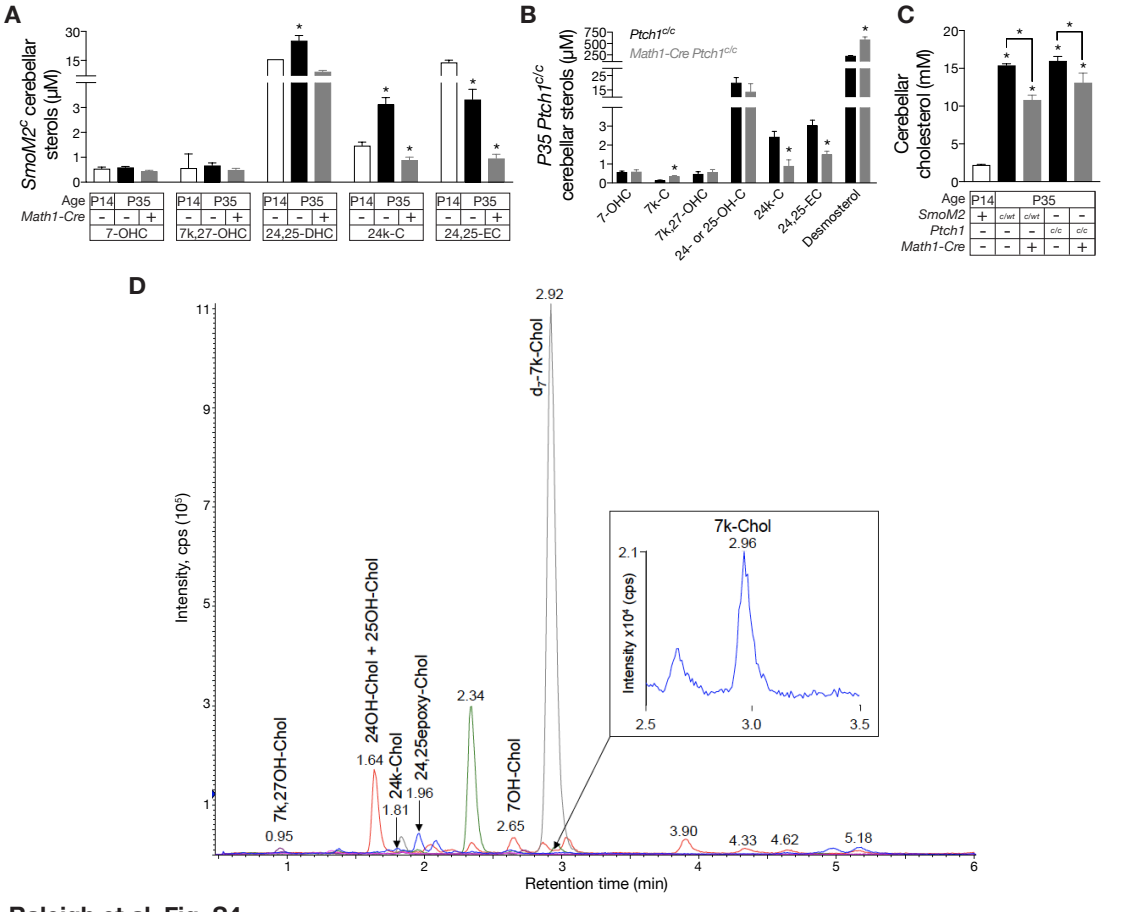

Raleigh et al. Fig. S4

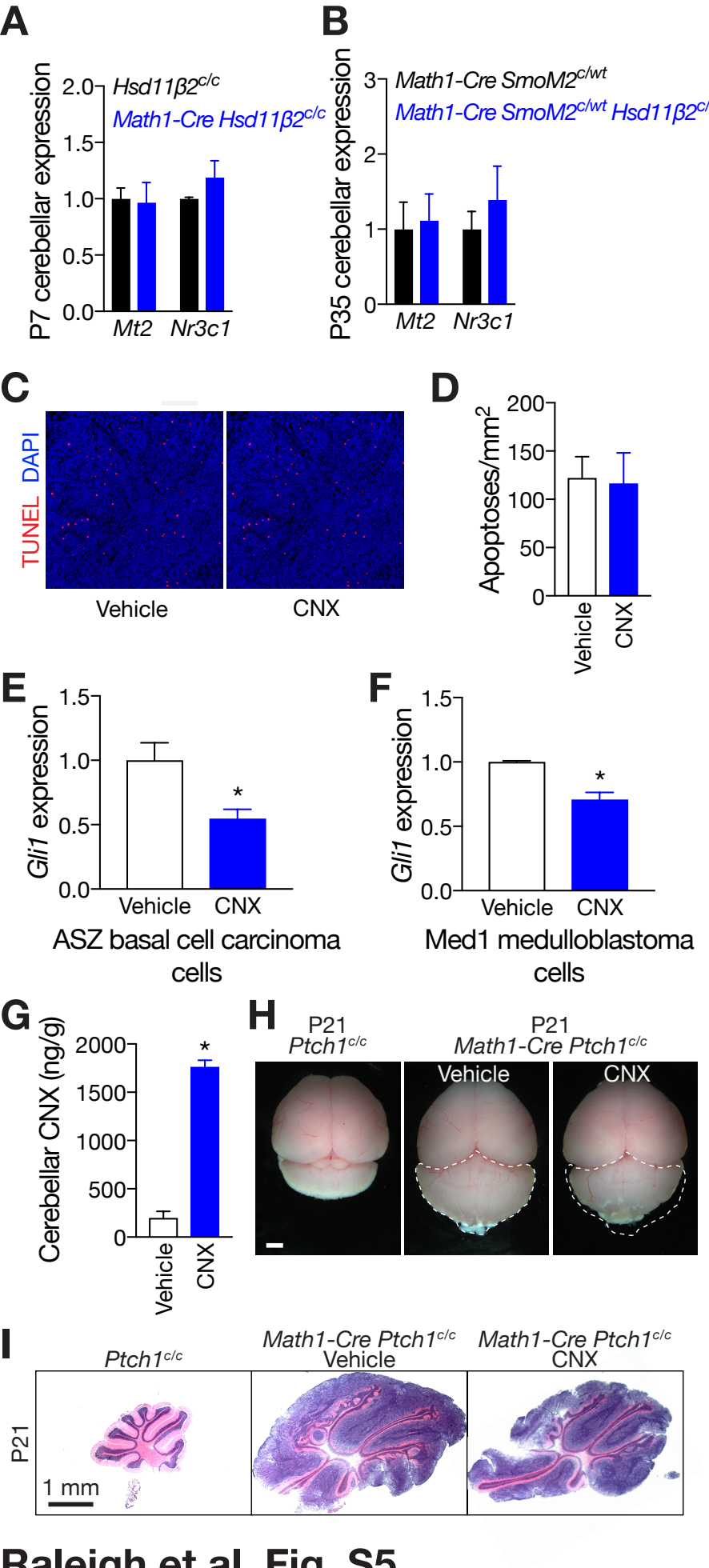

Raleigh et al. Fig. S5